Static correlations in macro-ionic suspensions: Analytic and numerical results in a hypernetted-chain—mean-spherical approximation

Sheema Khan, Thomas L. Morton, and David Ronis
Department of Chemistry, Harvard University, Cambridge, Massachusetts 02138
(Received 19 January 1987)

The static correlations in highly charged colloidal and micellar suspensions, with and without added electrolyte, are examined using the hypernetted-chain approximation (HNC) for the macro-ion—macro-ion correlations and the mean-spherical approximation for the other correlations. By taking the point-ion limit for the counter-ions, an analytic solution for the counter-ion part of the problem can be obtained; this maps the macro-ion part of the problem onto a one-component problem where the macro-ions interact via a screened Coulomb potential with the Gouy-Chapman form for the screening length and an effective charge that depends on the macro-ion—macro-ion pair correlations. Numerical solutions of the effective one-component equation in the HNC approximation are presented, and in particular, the effects of macro-ion charge, nonadditive core diameters, and added electrolyte are examined. As we show, there can be a strong renormalization of the effective macro-ion charge and reentrant melting in colloidal crystals.

I. INTRODUCTION

Spatial correlations in dilute, highly asymmetric electrolyte solutions (e.g., colloidal[1] or micellar[2] suspensions) pose a formidable challenge to modern liquid-state theories. The charge asymmetry is typically $O(10^2)$—$O(10^4):1$—2, and the macro-ion packing fractions are small. The theoretical difficulties are both conceptual and numerical. For example, some of the simpler analytic theories [e.g., the mean-spherical approximation (MSA)], if applied using physical parameters for the macro-ion charge and diameter, give only qualitative agreement with experiment or fail altogether. The reasons for the failure are the breakdown of the MSA at low density and its inability to correctly handle correlations in regions of strong electrostatic repulsion (e.g., negative pair correlations can result). Nonetheless, sometimes the Percus-Yevick or mean-spherical approximations can be solved analytically,[3] and this has led to several prescriptions for determining effective charge and diameters to use in MSA-based theories.[2,4–7]

While many of the problems associated with the MSA should be overcome when a more robust approximation such as the hypernetted-chain approximation (HNC) is used, there, one is faced with severe difficulties in obtaining a numerical solution to the nonlinear integral equations. As far as we are aware, this has limited the direct application of the HNC approach to systems where the charge ratio is less than 100:1 in the absence of added electrolyte,[8,9] although recently[10] a numerical analysis of a HNC—Percus-Yevick approximation for micelles has been reported.

The above-mentioned problems notwithstanding, it is well known that excellent fits to experimental structure factors for both colloidal and micellar suspensions can be obtained by using a one-component picture for the large ion with the Verwey-Overbeek[11] form for an effective macro-ion—macro-ion interaction potential, $U(r)$; i.e., with

$$U(r) \equiv U_{\text{s.r.}}(r) + \frac{e^2 z_{\text{eff}}^2 e^{-\lambda(r-\sigma)}}{\epsilon r} \quad \text{for } r \geq \sigma, \quad (1.1)$$

where $U_{\text{s.r.}}(r)$ is the nonelectrostatic (short-ranged) part of the macro-ion—macro-ion interaction potential, z_{eff} is an effective charge in electrons, e is the charge of an electron in electrostatic units, λ is the screening wave vector, σ is an effective macro-ion core diameter, and ϵ is the solvent dielectric constant. [Note, that in writing Eq. (1.1), we have incorporated an extra factor of $(1+\lambda\sigma/2)^2$ usually found in the denominator directly into the effective charge.] Once Eq. (1.1) is assumed, it is a simple matter to determine the structure factor within an approximate theory of the liquid state (e.g., HNC, MSA, etc.).

At present there are several theories that give prescriptions for determining the effective parameters or in mapping one approximate method onto another.[4–7] In particular, Hayter *et al.*[4(c)] have discussed ways of solving the effective one-component problem within the MSA, and Alexander *et al.*[12] have analyzed the effective charge within the nonlinear Poisson-Boltzmann equation. Finally, a variational principle based on the Gibbs-Bogoliubov inequality was used in Refs. 5 and 6 to determine effective sizes and effective charges, respectively.

In this work, we analyze and extend the possibility pointed out at the end of Ref. 6; namely, if counter-ions are assumed to have zero diameter, then Eq. (1.1) will be obtained as an exact consequence of a MSA closure on the counter-ion—counter-ion and counter-ion—macro-ion direct correlation functions no matter what approximation is used for the macro-ion—macro-ion correlations. This is true even if the counter-ion—macro-ion diameters are nonadditive, and, as we shall show in the next section, even if there are extra electrolytes in the solution. The macro-ion—macro-ion core diameter is not renormalized

and the screening length is that given by the Gouy-Chapman theory; however, there is a large change in the effective charge that is a functional of the macro-ion—macro-ion correlations through

$$\nu_0 \equiv 24\xi_{cc}\int_1^\infty dr\, re^{-\lambda(r-1)}g_{cc}(r)\,, \tag{1.2}$$

where $\xi_{cc} \equiv \pi\rho_c/6$ is the macro-ion packing fraction, $g_{cc}(r)$ is the macro-ion—macro-ion pair correlation function, and where we henceforth use units where the macro-ion—macro-ion core diameter is unity. Note, however, that in many cases, ν_0 is small and a simple analytic expression (which differs in the nonadditive diameter case from the Verwey-Overbeek[11] expression) is obtained.

In Sec. II, we extend the analysis of Ref. 6, to the case where more than one type of counter-ion is present and derive Eq. (1.1). In Sec. III, we numerically solve for the macro-ion correlations within the HNC approximation and compare the results with the experiments of Schaefer[1(d)] on colloids and with Chen *et al.*[2] on micelles. In addition, we analyze some of the general properties of the effective charge and compare with the results of Refs. 1(d), 2(b), and 9.

As we will show, the effective charge is in general less than the actual one. In general, the effect of the macro-ion—macro-ion Coulombic interaction goes through a maximum as the bare charge on the macro-ion is increased and then drops to zero (the rate depending on the degree of nonadditivity and the amount of added electrolyte). In particular, this gives the possibility of a certain type of reentrant behavior in colloidal crystals; namely, that the crystal will melt if the charge on the colloid is increased beyond a certain critical value. In our numerical analysis of the HNC equation, this possibility manifests itself as follows: as the charge on the colloid is increased, the height of the first peak in the structure grows until the Verlet criterion[13] for freezing is satisfied. Shortly thereafter, it becomes impossible to numerically solve the equations; however, if the region of extremely high charge is considered, then a solution to the equations is again found. This solution becomes more ideal gaslike as the charge on the macro-ion is increased. Moreover, if the charge on the macro-ion is decreased, then, as in the low charge region, the Verlet criterion followed by the inability to find a numerical solution will occur, thereby leaving a gap in the corresponding phase-diagram. This gap should correspond to the colloidal crystal phases. As we will see, the method works exceedingly well and numerical solutions for 1000:1 (on the low charge side) or 1 000 000:1 (on the high charge side) electrolyte solutions are easily obtained. Finally, in the last section, the results are summarized, the expected range of validity of the MSA-HNC theory is discussed, and some conjectures about the problems in the numerical methods are made.

II. THEORY

Interparticle correlations provide a valuable theoretical tool for probing the structure of a colloidal (or micellar) suspension that consists of macro-ions, associated counter-ions, and possibly added electrolyte. Such correlations can be described by the symmetrized form of the multicomponent Ornstein-Zernike equations:

$$h^s_{i,j}(r) = c^s_{i,j}(r) + \sum_{k=1}^{n} c^s_{i,k}(r) * h^s_{k,j}(r), \qquad i,j = 1,2,\ldots,n \tag{2.1}$$

where

$$h_{i,j}(r) = \frac{h^s_{i,j}(r)}{(\rho_i\rho_j)^{1/2}} \tag{2.2a}$$

and

$$c_{i,j}(r) = \frac{c^s_{i,j}(r)}{(\rho_i\rho_j)^{1/2}} \tag{2.2b}$$

are the usual pair and direct correlation functions, respectively, ρ_i is the density of species i, and $*$ denotes a convolution:

$$f*g \equiv \int d\mathbf{r}'\, f(\mathbf{r}')g(\mathbf{r}-\mathbf{r}')\,. \tag{2.3}$$

A full solution of the problem requires a second mathematical relation, or closure, between $c_{i,j}(r)$ and $h_{i,j}(r)$. It will be shown below that assumption of zero particle radius and the mean-spherical-approximation (MSA) for all species except the macro-ions, results in an effective one-component system interacting via a screened Coulomb potential. An interesting intermediate result is the transformation of the subset of all charged point-particle interactions into a mixture consisting of a neutral ideal gas and one component having an effective charge and density. It should be noted that the correlations of the transformed system are only mathematical constructs; the physical correlations of the counter-ions and electrolytes are recovered by inverting the transformation.

In keeping with the notation of Refs. 5 and 6, we henceforth denote macro-ion properties by the subscript c. The remaining electrolyes will be numbered from 1 to m, with 1 reserved for the original counter-ions of the macro-ion. Units are chosen such that the macro-ion—macro-ion core diameter is unity, and a common nonadditive point-ion—macro-ion diameter is denoted by R_{pc} ($R_{pc} \le \frac{1}{2}$). Furthermore, extensive use will be made of the electroneutrality relations associated with both the macro-particle and the added salt:

$$\rho_c z_c + \rho_1 z_1 = 0 \tag{2.4a}$$

and

$$\sum_{k=2}^{m} \rho_k z_k = 0\,, \tag{2.4b}$$

where z_i is the charge of species i. The macro-ion—point-particle form of the Fourier-transformed Ornstein-Zernike equations can be written in the following matrix notation:

$$\underline{\mathbf{H}}(k) = (1 + \tilde{h}^s_{c,c})\underline{\mathbf{T}}(k) + \underline{\mathbf{C}}(k)\,\underline{\mathbf{H}}(k)\,, \tag{2.5}$$

where matrices have underlines,

$$[\underline{\mathbf{H}}]_i(k) \equiv \tilde{h}^s_{c,i}(k), \quad i = 1,2,\ldots,m \tag{2.6a}$$

$$[\underline{T}]_i(k) \equiv \tilde{c}^s_{c,i}(k), \quad i=1,2,\ldots,m \tag{2.6b}$$

$$[\underline{C}]_{i,j}(k) \equiv \tilde{c}^s_{i,j}(k), \quad i,j = 1,2,\ldots,m \tag{2.6c}$$

and where the Fourier transform is defined by

$$\tilde{f}(\mathbf{k}) \equiv \int d\mathbf{r}\, e^{i\mathbf{k}\cdot\mathbf{r}} f(\mathbf{r}) \,. \tag{2.7}$$

The eigenvalues and eigenvectors of $\underline{C}$ depend on the particular closure chosen for this subset of correlations. One possibility is the MSA; i.e.,

$$c_{i,j}(r) = -\beta u_{i,j}(r), \quad r > R_{i,j} \tag{2.8a}$$

and

$$h_{i,j}(r) = -1, \quad r < R_{i,j} \tag{2.8b}$$

where $u_{i,j}(r)$ is the interaction potential between species i and j. For point ions,

$$c_{i,j}(r) = -\frac{\beta e^2 z_i z_j}{\epsilon r}, \quad r>0 \tag{2.9}$$

where $\beta = (k_B T)^{-1}$. This implies that

$$[\underline{C}(k)]_{i,j} = -\frac{Q_i Q_j}{k^2} \,, \tag{2.10}$$

where

$$Q_i \equiv \left[\frac{4\pi\beta e^2 \rho_i}{\epsilon}\right]^{1/2} z_i \,. \tag{2.11}$$

It is easily seen from Eq. (2.10) that $\underline{C}$ has only one independent column-vector, implying that it has only one nonzero eigenvalue, α, equal to its trace; i.e.,

$$\alpha \equiv -\left[\frac{\lambda}{k}\right]^2 = -\sum_{i=1}^{m} \frac{Q_i^2}{k^2} \,, \tag{2.12}$$

where λ is the Debye screening wave vector. By using Eq. (2.10), $\underline{C}$ is easily diagonalized; i.e.,

$$\underline{C}'(k) \equiv \underline{P}^{-1}\underline{C}(k)\underline{P} \,, \tag{2.13}$$

where

$$[\underline{C}'(k)]_{i,j} = -\frac{\lambda^2}{k^2}\,\delta_{i,1}\delta_{j,1} \,, \tag{2.14}$$

and

$$[\underline{P}]_{i,j} = \frac{Q_i}{\lambda}\,\delta_{j,1} - \frac{(1-\delta_{j,1})(\delta_{i,1}Q_j - \delta_{i,j}Q_1)}{(Q_j^2 + Q_1^2)^{1/2}} \tag{2.15}$$

is an orthonormal transformation. Henceforth, $\delta_{i,j}$ denotes the Kronecker-delta. The inverse Fourier transform of Eq. (2.14), i.e.,

$$(c^s_{i,j})'(r) = -\frac{\lambda^2}{4\pi r}\,\delta_{i,1}\delta_{i,j}, \quad r > 0 \tag{2.16}$$

implies that the subsystem of point-ions is equivalent to a mixture of neutral-point gases and a one-component plasma. The former have a zero effective potential, and the latter interacts via a Coulomb potential. The effective charge of the plasma is not exactly $\lambda/(4\pi)^{1/2}$, since the symmetrized correlations incorporate an effective density that is yet to be determined. All properties associated with the effective point-ion species will be denoted by a subscript p as was done in Refs. 5 and 6.

By noting that $\underline{P}^{-1} = \underline{P}^T$ (the superscript T denotes the transpose), and left multiplying Eq. (2.5) by $\underline{P}^T$ we find that

$$\underline{H}'(k) = [1 + h^s_{c,c}(k)]\underline{C}'(k) + \underline{C}'(k)\underline{H}'(k) \,, \tag{2.17}$$

where the vectors transform as:

$$\underline{F}' = \underline{P}^T\underline{F} \,. \tag{2.18}$$

Furthermore, by assuming the MSA closure for all macro-ion—counter-ion correlations [cf. Eq. (2.8)], it follows that

$$(c^s_{c,p})'(r) = -\frac{Q_c\lambda}{4\pi r}, \quad r > R_{pc} \tag{2.19a}$$

and

$$(c^s_{c,j})'(r) = 0, \; r > R_{pc}, \; j = 2,3,\ldots,m \,. \tag{2.19b}$$

The above equations are consistent with the physical interpretation of Eq. (2.14): the effective interactions outside the core vanish for the case of the neutral-point components, while the point-ion—macro-ion forces are electrostatic in nature. The transformed assembly of particles is completely characterized by effective charges and densities.

From Eqs. (2.11), (2.12), and (2.19a), it follows that

$$z_p = \left[\frac{\sum_{i=1}^{m}\rho_i z_i^2}{\rho_p}\right]^{1/2} ; \tag{2.20}$$

hence, all that remains to be evaluated are the effective densities. These are easily obtained by evaluating $h^{s'}_{c,i}$ [cf. Eqs. (2.17) and (2.18)] within the core, and comparing the transformed functions to the closure relation (2.8b). It follows that the effective point-ion density is

$$\rho_p = \frac{(\rho_1 z_1)^2}{\left[\sum_{i=1}^{m}\rho_i z_i^2\right]} \,, \tag{2.21a}$$

while the effective densities of the $m-1$ neutral-point components are

$$\rho'_i = \frac{[Q_1(\rho_i)^{1/2} - Q_i(\rho_1)^{1/2}]^2}{(Q_i^2 + Q_1^2)}, \quad i = 2,3,\ldots,m \,. \tag{2.21b}$$

Since the various neutral-point components are physically equivalent, in effect, there is only one neutral-point component whose properties (denoted by subscript n) are obtained by the simple superposition of the corresponding $m-1$ independent quantities. In particular,

$$\rho_n = \sum_{i=2}^{m}\rho'_i \,, \tag{2.22a}$$

$$c^s_{j,n}(r) = \sum_{i=2}^{m} c^{s'}_{i,j}(r), \quad j = c,p \tag{2.22b}$$

and

$$h^s_{j,n}(r) = \sum_{i=2}^{m} h^{s'}_{i,j}(r), \quad j = c,p \ . \tag{2.22c}$$

Finally, it is straightforward to verify electroneutrality in the transformed system by using Eqs. (2.20) and (2.21a):

$$\rho_p z_p + \rho_c z_c = 0 \ . \tag{2.23}$$

At this point it is useful to rewrite the transformed, three-component (symmetrized) Ornstein-Zernike equations, along with the MSA closure:

$$h^s_{i,j}(r) = c^s_{i,j}(r) + \sum_{k=p,c,n} c^s_{i,k}(r) * h^s_{k,j}(r) \ , \tag{2.24}$$

$$c^s_{i,j}(r) = -\frac{Q_i Q_j}{4\pi r}, \quad r \geq R_{i,j} \tag{2.25a}$$

and

$$h^s_{i,j}(r) = -(\rho_i \rho_j)^{1/2} \text{ for } r \leq R_{i,j} \ , \tag{2.25b}$$

where $i,j = p,c,n$, except for $i = j = c$.

We have recently analyzed this three-component problem[6] and a summary of the solution to Eqs. (2.25a)–(2.25c) is now presented. As we have shown in Ref. 6, the three-component system can be successively reduced to a two- and finally a one-component system. The only nonvanishing neutral-point components direct correlation is constant within the core; specifically,

$$c^s_{n,c}(r) = \frac{(\rho_c \rho_n)^{1/2}}{(\xi_{nc} - 1)}, \quad r \leq R_{p,c} \tag{2.26}$$

where $\xi_{nc} \equiv 4\pi\rho_c R^3_{pc}/3$ is the neutral–macro-ion packing fraction. The two-component macro-ion–macro-ion direct correlation function, $c^{(2)}_{c,c}(r)$, is related to $c_{c,c}(r)$ according to:

$$c^s_{c,c}(r) = c^{s\,(2)}_{c,c}(r) - c^s_{n,c}(r) * c^s_{n,c}(r) \ . \tag{2.27}$$

It is easily shown that the second term vanishes for $r \geq 2R_{pc}$. The restriction $2R_{pc} \leq 1$ guarantees that $c^{(2)}_{c,c}$ can be chosen such that the core condition is satisfied. Examination of the $h_{p,c}$ Ornstein-Zernike equation within the core shows that

$$c^{(2)}_{p,c}(r) = c_{p,c}(r) \equiv \Gamma \text{ for } r \leq R_{pc} \ , \tag{2.28}$$

where

$$\Gamma = \frac{\beta e^2 z_c z_p \{\lambda^2[\nu_0 e^{-\lambda}\cosh(\lambda R_{pc}) - \lambda e^{-\lambda R_{pc}}] - 4\pi\rho_c\} - \epsilon\lambda^2}{\epsilon\lambda\{\nu_0 e^{-\lambda}[\sinh(\lambda R_{pc}) - \lambda R_{pc}\cosh(\lambda R_{pc})] + \lambda(1 + \lambda R_{pc}) e^{-\lambda R_{pc}}\}} \ , \tag{2.29}$$

and where ν_0 is given by Eq. (1.2). The Fourier transform of an effective one-component direct correlation function, $\tilde{c}^{(1)}_{c,c}(k)$ is related to the two-component direct correlation functions by

$$\tilde{c}^{s(1)}_{c,c}(k) = \tilde{c}^{s(2)}_{c,c}(k) + \frac{[\tilde{c}^s_{p,c}(k)]^2}{1 - \tilde{c}^s_{p,p}(k)} \ . \tag{2.30}$$

By using the Fourier transforms of Eqs. (2.25a) and (2.28) for $\tilde{c}^s_{p,c}(k)$ and $\tilde{c}^s_{p,p}(k)$, inverting the above equation for $r \geq 1$ gives

$$c^{(1)}_{c,c}(r) = c^{(2)}_{c,c} + \frac{\beta e^2 z_c^2}{\epsilon r} - \frac{\Omega e^{-\lambda(r-1)}}{r} \quad \text{for } r \geq 1 \ , \tag{2.31}$$

where

$$\Omega = \frac{\beta e^2 z_c^2 \, e^{-\lambda}}{\epsilon} \left[\frac{\lambda}{C\nu_0 + D}\right]^2 , \tag{2.32}$$

$$C \equiv e^{-\lambda}[\sinh(\lambda R_{pc}) - \lambda R_{pc}\cosh(\lambda R_{pc})] \ , \tag{2.33a}$$

and

$$D \equiv \lambda e^{-\lambda R_{pc}}(1 + \lambda R_{pc}) \ . \tag{2.33b}$$

Note that the extra factor of ρ_c has been dropped in writing Eqs. (2.31) and (2.32). The expression for the contact potential, Ω, is identical to that obtained previously by the full MSA[6] analysis; however, its value will differ depending on the macro-ion–macro-ion closure used to compute ν_0. Note that λ does not explicitly include the ionic strength of the macro-ions; nonetheless, it is easy to show that the correlations will decay with the usual Debye screening length (i.e., including the macro-ions) when the low charge and density limit is taken.

Equation (2.31) is the key result of this section. Moreover, in obtaining this result, we did not use the closure for the macro-ion–macro-ion direct correlations. This is fortunate because the MSA will break down outside the core in regions where the potential is large, and this will occur for the macro-ion–macro-ion correlations long before the p-p or c-p correlations.

An approximation which should be better able to deal with the strong interactions associated with the macro-ion–macro-ion Coulomb repulsions is the hypernetted chain approximation (HNC);[14] i.e.,

$$h_{c,c}(r) = \exp[-\beta u_{c,c}(r) + h_{c,c}(r) - c_{c,c}(r)] - 1 \ , \tag{2.34}$$

where we recall that $c_{c,c}(r)$ is the macro-ion–macro-ion direct correlation function including the explicit effects of the other ions. However, if the MSA is invoked for the other ions, then Eqs. (2.27) and (2.31) can be used to reduce the problem to one for a single-component system. Specifically, Eq. (2.34) becomes

$$h_{c,c}(r) = \exp\left[-\beta u_{c,c}(r) + \frac{\beta z_c^2 e^2}{\epsilon r} + h_{c,c}(r) - c_{c,c}^{(1)}(r) - \frac{\Omega e^{-\lambda(r-1)}}{r}\right] - 1 , \quad (2.35)$$

where we recall that $h_{c,c}$ and $c_{c,c}^{(1)}$ are related by the one-component Ornstein-Zernike equation:

$$h_{c,c}(r) = c_{c,c}^{(1)}(r) + \rho_c\, c_{c,c}^{(1)} * h_{c,c} . \quad (2.36)$$

The Coulomb part of the macro-ion—macro-ion potential is canceled by the second term in the exponent in Eq. (2.35) leaving only the short-ranged part, $u_{s,r}(r)$. The multicomponent ionic solution problem has thus been transformed into a one component problem for a macro-ionic suspension interacting via a screened Coulomb potential. It is interesting to note that this is the starting point of many calculations of the structure factors of macro-ionic suspensions,[2,4] although here the strength of the Yukawa interaction depends on $h_{c,c}$ through Eq. (2.32).

It is useful to rewrite Eq. (1.2) as

$$\nu_0 \equiv 24\xi_{cc}\left[\lambda^{-1} + \lambda^{-2} + \int_1^\infty dr\, r e^{-\lambda(r-1)} h_{cc}(r)\right] . \quad (2.37)$$

For sufficiently low density, the integral on the right-hand side of Eq. (2.37) will be very small; furthermore, the first two terms will also be unimportant when the screening length is not too long. In this event,

$$\Omega \approx \frac{\beta e^2 z_c^2 e^{-\lambda(1-2R_{pc})}}{\epsilon(1+\lambda R_{pc})^2} . \quad (2.38)$$

An effective charge, z_c^{eff} can be identified from Eq. (2.38) as

$$z_c^{\text{eff}} = z_c e^{-\lambda(1/2-R_{pc})}/(1+\lambda R_{pc}) .$$

This expression is a generalization of the linearized Verwey-Overbeek theory,[11] but differs by the presence of the exponential and the factor in the denominator containing R_{pc} instead of $\frac{1}{2}R_{cc}$. In the additive case, the two are equivalent. Note, however, that the general expression, Eq. (2.32), is quite different than the full Verwey-Overbeek expression.[11] We now present some numerical examples.

III. RESULTS

A. Colloids

Numerical solutions of the HNC equation often fail to converge for small hard-spheres with charge exceeding $100e$ due to the strength of Coulombic interactions at or near contact. However, the combination of the closed, self-consistent form of the screened-Coulomb potential [cf. Eq.(2.31)], along with the algorithm developed by Gillan[15], has made it easy to solve the effective one component MSA-HNC equations for suspensions with experimental charges exceeding $10^4 e$.

Gillan's method uses a Newton-Raphson algorithm to determine the gross structural features of $\gamma(r) \equiv h(r)-c(r)$ (as represented by a finite number of basis functions), and a Picard iteration to determine the finer structure of $\gamma(r)$. For basis functions, we use the roof functions described in Ref. 15. We used ten functions, whose range extended to beyond the point where $\gamma(r) < 0.1$. The Fourier transforms were performed by the fast Fourier transform technique, using 2048 grid points. The integrals were cut off at ten times the minimum of $\rho_c^{-1/3}$ and the distance where the screened Coulomb potential equals $k_B T$.

In light scattering experiments conducted by Brown *et al.*[1(b)] on five suspensions of identical colloid charge ($z_c = 582e$) and diameter ($R_{cc} = 500$ Å), the maximum peak position was found consistently at $1.1 \times 2\pi(\rho_c)^{1/3}$. Such scaling of the peak position was also observed for dilute suspensions studied by Schaefer;[1(d)] in particular, Fig. 1 illustrates the insensitivity of the maximum peak position to changes in the colloidal charge (in keeping with the density scaling behavior). Furthermore, the local order [e.g., as characterized by the height in the first maximum of $S_{cc}(k)$] increases as the charge is increased, culminating in a liquidlike structure factor which is close to the experimental data. Note that the latter does not approach the correct asymptotic value of 1 for $kR_{cc} \gg 1$ as required by the definition of $S(k)$. In any case, the fitted charge ($z_c = 400e$) lies well within the margin of error of the reported value ($z_c^{\text{expt}} = 432 \pm 100e$).

Although the reported experimental conditions[1(d)] excluded the presence of added electrolytes, Fig. 2 illustrates

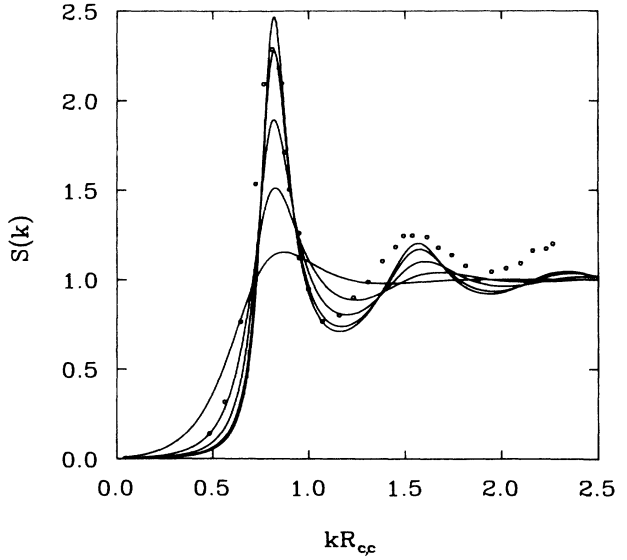

FIG. 1. Colloid-colloid structure factors for a suspension containing 2.56×10^{12} 872-Å-diameter colloid particles per cm^3 in water at 46 °C. The solid curves show the effect of changing the charge on the colloid and correspond to $z_c = 450$, 400, 300, 200, and 100 electrons [in order of decreasing height of the first maximum of $S(k)$]. The discrete points are the experimental points of Schaefer [Ref. 1(d)].

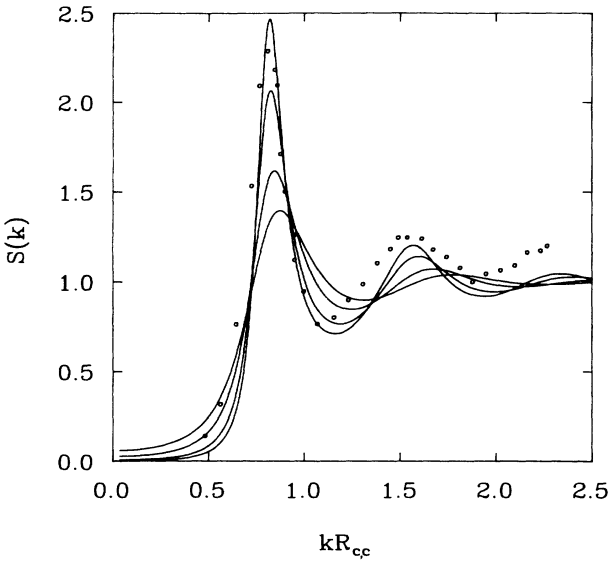

FIG. 2. The effect of changing the screening length by adding salt for the 450 electron case shown in Fig. 1. The various curves correspond to 0×10^{-6} M, 1×10^{-6} M, 3×10^{-6} M, and 5×10^{-6} M concentration of added 1-1 electrolyte [in order of decreasing height of the first maximum of $S(k)$].

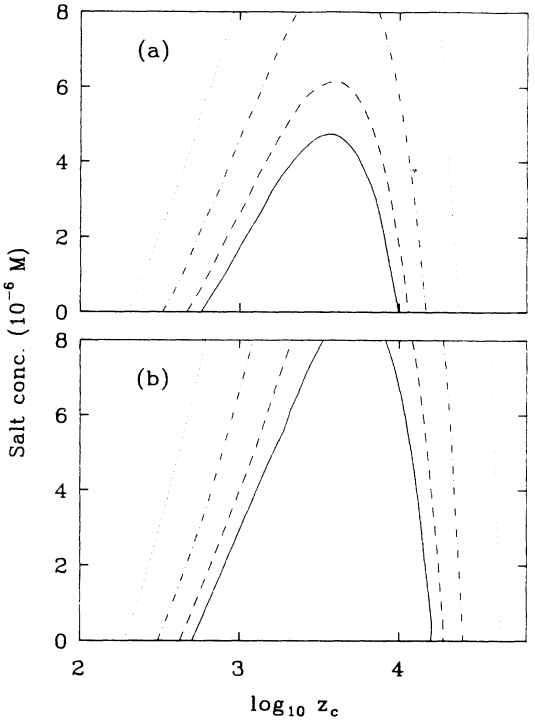

FIG. 3. The effects of charge and added salt on the height of the first maximum S_{cc} for R_{cc} = 872 Å (panel a) and 2340 Å (panel b). In each case, the colloid number density was 2.56×10^{12} cm^{-3} at 46°C. The contours are at S_{cc} = 1.5 (· · · ·), 2.0 (—·—·—·), 2.5 (— — —), and 2.85 (——).

the dramatic effect of the addition of micromolar amounts of 1-1 electrolyte on the maximum peak height. This result should not be surprising for dilute systems where the counter-ion concentration is also in the micromolar regime; e.g., the addition of 1×10^{-6} M of 1-1 electrolyte decreases the screening length by a factor of $2^{1/2}$.

Such behavior is relevant to the phase transitions of extremely dilute, highly-charged colloidal suspensions from the crystalline phase to the liquid state. In the absence of added electrolyte, a liquidlike suspension should crossover into the crystalline phase once a critical charge is exceeded. However, if the charge is increased further, a second critical value is attained when the large density of neutralizing counter-ions screens out the electrostatic repulsions, and the colloidal crystal will melt. These physical arguments are manifest mathematically in Eq. (2.31); the leading-order behavior of the interaction for $\lambda \to \infty$ is a balance between the competing factors $(z_c/\lambda)^2$ and $e^{-\lambda(r-2R_{pc})}$ $(\lambda\sim z_c)^{1/2}$ as $z_c \to \infty$. Once the second critical charge is exceeded, the strength of the interaction is governed by the exponential factor, and in the limit of infinite charge, the colloidal suspension can be modeled as an extremely dilute solution of hard spheres.

The fine balance between screening and electrostatic repulsions can be altered in favor of the former by the addition of electrolytes. With reference to colloidal crystallization, the presence of micromolar concentrations of salt should dramatically reduce, and possibly even eliminate, the range of existence of the crystalline phase. A quantitative analysis of this is shown in Figs. 3 and 4.

Each phase diagram has been constructed by plotting contours of the maximum peak height, S_{max}, as a function of colloid charge and added salt concentration. The region enclosed within the Verlet[13] criterion contour, S_{max} = 2.85, represents the crystalline phase. The contour map shown in Fig. 3(a) is based on the colloidal density and diameter reported by Schaefer;[1(d)] both the experimental point (z_c = 432e; no salt) and the refitted HNC value (z_c = 400e; no salt) lie to the left of the Verlet contour. Since the maximum number of ionizable head groups per colloid is 3040e, [1(d)] observation of a reentrant-liquid (predicted at $z_c \approx 10^4$) is impossible, al-

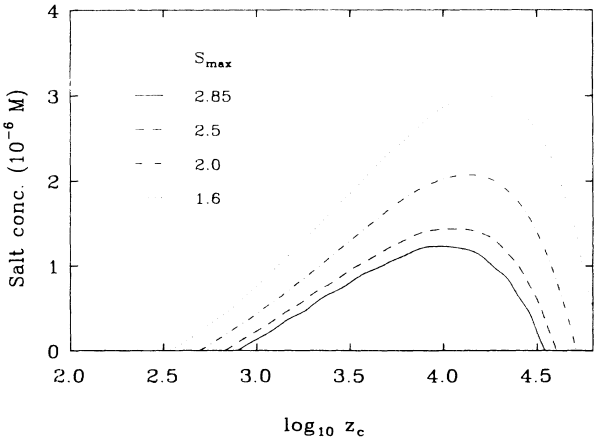

FIG. 4. Same as Fig. 3(b), but now, the colloid density is 1.41×10^{11} cm^{-3}.

though a transition from liquid to crystalline phases should occur as the colloid charge approaches $625e$. Furthermore, this transition can be eliminated altogether by the addition of salt in excess of 5×10^{-6} M.

Structural changes can be induced by variation of not only charge and salt concentration, but by the colloid diameter as well. For the same total charge, larger colloids have smaller surface charge density and thus the counterions will be less tightly bound to the colloid surface; this is equivalent to increasing the effective charge of the colloid. Since there is an enhancement of local order as the macro-ionic diameter is increased, the relative change in λ must be greater in order to screen out the interparticle interactions. This is demonstrated by Fig. 3(b), where the colloid size has been increased by a factor of 2.7 over that used to construct Fig. 3(a) (the number density is the same). The upward elongation of the contours reflects the fact that at a given charge, a greater concentration of electrolyte is required to reduce the correlations in the larger diameter system. The shift of the reentrant phenomena to higher charge is a manifestation of the same effect: a greater density of counter-ions is required to screen out the enhanced interactions of the 2340-Å system.

Finally, a phase diagram for the suspension parameters reported by Clark and Ackerson[1(c)] ($\xi_{cc}=9.5\times10^{-4}$, $R_{cc}=2340$ Å) is presented in Fig. 4. From the definition of λ [cf. Eq. (2.12)], it is easily seen that the relative effect of added electrolyte is enhanced as the suspension becomes increasingly dilute. Since the packing fraction is even less than that of the previous case, the crystalline phase ceases to exist for salt concentrations in excess of $1\times10^{-6}M$. Note that the experimental point ($z_c = 12\,700e$, no salt) lies within the Verlet-criterion contour, whereas light-scattering experiments show the system to be in the liquid state. This discrepancy can be accounted for in one of three ways: (i) the charge is correct, while the assumption of the absence of stray electrolyte is not, (ii) the reported charge is too low (if the latter is true, then it should be possible to observe reentrant behavior in the reverse direction by reducing the colloidal charge), or (iii) the MSA is breaking down for the macro-ion—counter-ion correlations.

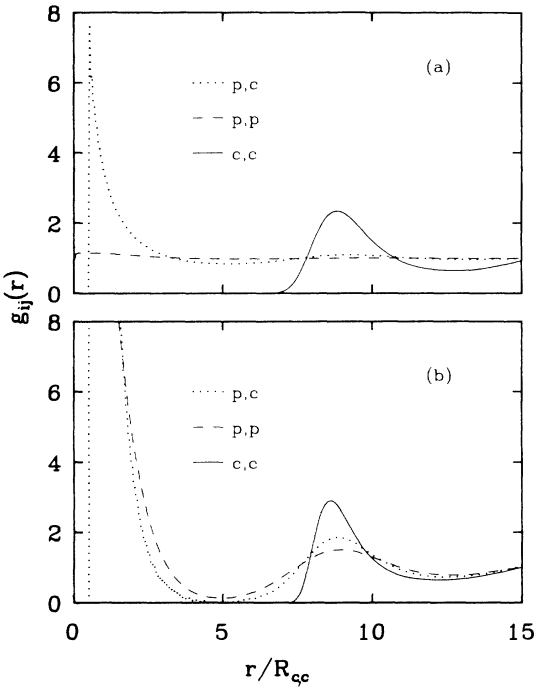

FIG. 5. Pair correlation functions for colloidal suspensions containing 2.56×10^{12} cm^{-3} 872-Å-diameter particles in water at 46°C. $z_c = 500e$ in panel (a) and $11\,000e$ in panel (b). Note that the maximum values for g_{pc} and g_{pp} in panel (b) were 104.3 and 22.3, respectively.

The pair correlation functions for two systems on either side of the two-phase region in Fig. 3(a) (no added salt) are shown in Fig. 5. Panels 5(a) and 5(b) correspond to colloid charges of 500 and $11\,000e$, respectively. The charges were chosen to give S_{cc}'s with comparable maximum values (~2.6), and indeed, the corresponding $g_{cc}(r)$'s are similar.

Once the macro-ion—macro-ion structure factor is obtained, it is a simple matter to obtain the other partial structure factors. From Eqs. (2.24) and (2.28), it follows that

$$S_{pc} = 4\pi(\rho_c\rho_p)^{1/2}\left[\frac{\Gamma}{k}[\sin(kR_{pc})-kR_{pc}\cos(kR_{pc})]-\frac{\beta e^2 z_p z_c}{\epsilon}\cos(kR_{pc})\right]\frac{S_{cc}(k)}{k^2+\lambda^2} \tag{3.1a}$$

and

$$S_{pp}(k) = \frac{k^2}{k^2+\lambda^2} + \frac{S_{pc}^2(k)}{S_{cc}(k)} . \tag{3.1b}$$

The other correlations show three main features: (1) a large positive p-c pair correlation at R_{pc}, (2) induced correlations in g_{pp} and g_{pc} at the maximum of g_{cc}, and (3) induced correlations in g_{pp} at R_{pc}. In all cases, the correlation functions were positive, although (see below) in the MSA this need not be the case. Note, that the maximum heights of g_{pc} and g_{pp} increase with increasing charge, reflecting the increased density of counter-ions near a given colloid. Figure 6 shows S_{pc} for $z_c = 11\,000e$. Notice, as expected from Fig. 5(b), the presence of two characteristic length scales.

B. Micelles

Treatment of the counter-ions as point particles is not only mathematically appealing, but intuitively reasonable

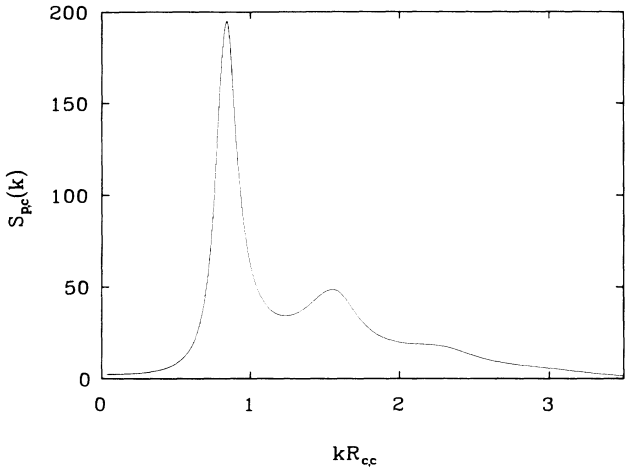

FIG. 6. S_{pc} for the case shown in 11 000e case Fig. 5(b).

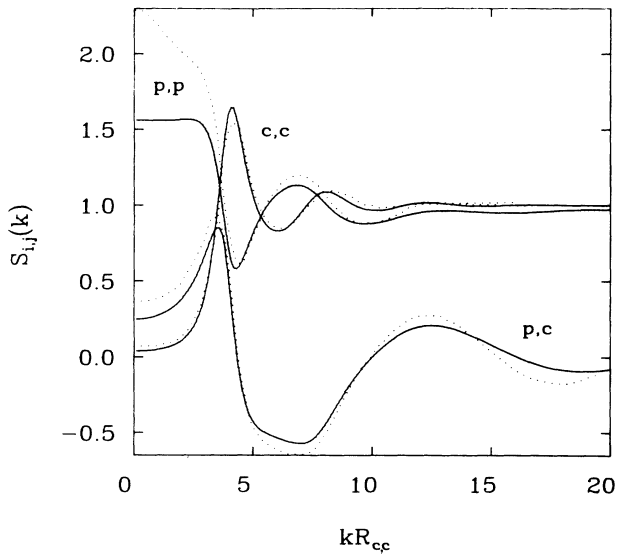

FIG. 7. Partial structure factor for a 0.0025M micellar suspension in water at 298 K. The charge ratio was 40:1 and R_{cc} = 50 Å. The solid curves are the results of the MSA-HNC approximation and the dotted curves are the results of the Belloni's multicomponent HNC calculation (Ref. 9). Note that the latter assumed additive diameters with R_{pp} = 5 Å.

for dilute colloidal suspensions where the ratio R_{cc}/R_{pp} ranges from 10^2 to 10^3. It has already been shown in a Percus-Yevick analysis[5] of these systems that the size of the counter-ion is of minimal importance for the calculation of the colloid-colloid structure factor. This feature is also manifest experimentally by the position of the first peak, which scales according to the density, rather than the size of the colloid. The final justification of this approximation for colloids is illustrated by Fig. 1 where excellent agreement with the observed structure factor is obtained.

The success of the point-ion approximation should not be automatically precluded for micellar suspensions where typically $R_{cc}/R_{pp} = 10$. However, by using a multicomponent HNC closure for the primitive electrolyte model with parameters which are typical of micellar suspensions, Belloni[9] has shown that the micelle-micelle correlations are insensitive to variation of the counter-ion diameter from 0–5 Å.

Figure 7 compares the micelle-micelle and micelle—counter-ion structure factors obtained by the relatively simple MSA-HNC point-ion approximation, with their respective counterparts obtained by the full HNC finite-size counter-ion study of Belloni. Given that both theories satisfy the Stillinger-Lovett electroneutrality condition,[16] i.e.,

$$\sum_{i=p,c} \rho_i z_i S_{ij}(k=0) = -z_j, \quad j = p,c \tag{3.2}$$

the small discrepancy between the two $S_{pc}(k=0)$ values is magnified by a factor of $z_c^{1/2} \sim 6.3$ when comparing the two $S_{pp}(k=0)$ values. In addition, it is well known that the MSA can give negative pair correlation functions. This is the case here for $g_{pp}(r)$ and this will reduce the value of $S_{pp}(k=0)$. However, $g_{pp}(r)$ is negative only for very small separations, and as is shown in Fig. 8, this does not have a large effect on the correlations outside the macro-ion core.

By comparing the two $g_{pc}(r)$ maxima [$g_{pc,\mathrm{HNC}}(r=R_{pc})=11.3$ and $g_{pc,\mathrm{MSA\text{-}HNC}}(r=R_{pc})=4.3$], it is seen that the counter-ion—micelle correlation is stronger when approximated by the HNC approximation (which treats the Coulomb interaction in a more nonlinear manner than the MSA). Consequently, there is a greater density of counter-ions in the vicinity of a given micelle, implying that macro-ion correlations in the MSA-HNC approximation will be stronger than in the full HNC approximation. This is reflected in Fig. 8 by the slightly larger first maximum of the MSA-HNC macro-ion—macro-ion pair correlation function.

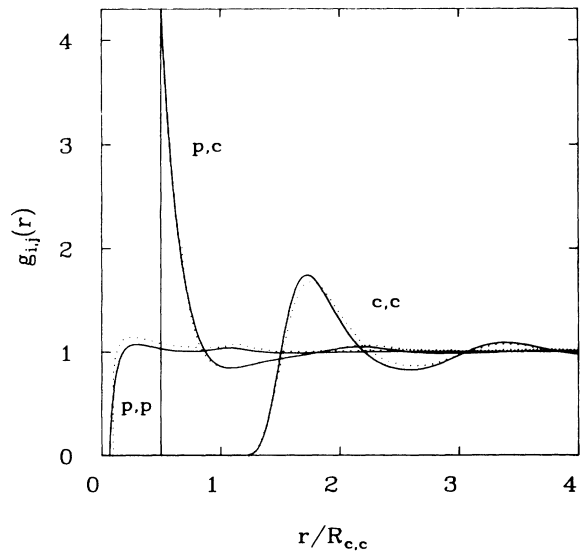

FIG. 8. Pair correlation functions for the system shown in Fig. 7.

In addition, four micellar suspensions were examined,[2(b)] with the experimental parameters lying in the following ranges: $0.015 \lesssim \xi < 0.14$; $53 < z_c < 75$; and 44.3 Å $< R_{cc} <$ 48.4 Å. According to Fig. 9, the maximum of each of the theoretical micelle-micelle structure factors are consistently too high and occur at too low a wavenumber compared to their experimental counterparts. Since the peak positions scale approximately as $1.1 \times 2\pi(\rho_c)^{1/3}$, the latter can be interpreted to mean that the micellar density is somehow underestimated, while the former implies that the micellar interactions are not sufficiently screened. In many cases, the experimental structure factors were fit to the raw scattering intensity data by assuming that peak position scales according to the micellar diameter; however, by analogy with colloidal suspensions, $1.1 \times 2\pi(\rho_c)^{1/3}$ is an equally possible characteristic wavenumber. With this in hand, it is possible to reinterpret the scattering intensity data while maintaining the microscopic model assumed by Chen[2(b)] in the lithium dodecyl sulfate (LDS) system. A brief summary of the latter is presented below.

As is well known,

$$I(k) \propto \rho_c P(k) S_{cc}(k) , \tag{3.3}$$

where P(k) is a form factor specific to the assumed geometry of the micelle, and $S_{cc}(k)$ is the intermicellar structure factor. The fitting procedure thus requires the use of a theoretical model for the micellar shape (spherical), and a choice of an *approximate* theory for the structure factor. The internal micellar structure was modeled as a spherical hydrocarbon core, of radius R_{core} and ionic head groups, each of diameter 5.56 Å,[2(b)] attached to the surface of the core. The micellar diameter is therefore:

$$R_{cc}^{(0)} = 2(R_{\text{core}} + 5.56 \text{ Å}). \tag{3.4a}$$

Each head group carries a unit charge. If the total LDS monomer concentration is fixed and complete micellization is assumed, it follows that micellar charge and density are inversely related; i.e., $z_c \propto \rho_c^{-1}$. Furthermore, for constant core density, the charge (or aggregation number) is the ratio of the core volume to the monomer volume, implying that $z_c \propto R_{\text{core}}^3$. Since the neutrons scatter mainly off of the hydrocarbon core, the form factor (for spherical geometry) is related to the core size according to

$$P(k) \propto \left[\frac{V_c j_1(kR_{\text{core}})}{kR_{\text{core}}} \right]^2 , \tag{3.4b}$$

where V_c is the core volume, and $j_1(x)$ is the first-order spherical Bessel function. Hence,

$$I(k) \propto \rho_c \left[\frac{R_{\text{core}}^2 j_1(kR_{\text{core}})}{k} \right]^2 S_{cc}(k) . \tag{3.5}$$

We now refit the experimental data by: (1) assuming that the aggregation number or $z_c \propto R_{\text{core}}^3$ with the proportionality constant of Chen *et al.*[2(b)] and (2) allowing for partial micellization. The free ionized monomers are then approximated as excess point salt-ions; these enhance the screening of the interaction between micelles and reduce the height of the intensity maximum. In addition, no explicit correction for the CMC is made; the density of unmicellized monomer plus the density of monomer within the micelles is equal to the total density of LDS.

The degree of micellization and charge per micelle were varied until the best fit to the scattering intensity was obtained and the improvement of $I(k)$ over that obtained by using the reported parameters is shown in Fig. 9. Note that the two most dilute solutions exhibit theoretical intensities with distinct shoulders, indicative of enhanced second peak of S_{cc}. In addition, these last two cases have theoretical intensities which are much smaller than the experimental ones at small scattering wave numbers. This reflects the small values of $S_{cc}(k=0)$ obtained within the HNC approximation.

The absence of such features in the experimental data can be explained by a number of mechanisms. First, polydispersity[17] leads to the averaging of several structure factors and can result in the observed smooth tail. Second, it has been suggested[18] that the secondary structure in $I(k)$, obtained theoretically [see, e.g., Figs. 9(c) and 9(d)], is a result of neglecting the scattering from the monomer head group region. This effect can be incorporated into the form factor as the difference $[R_{\text{core}}^2 j_1(kR_{\text{core}})/k]^2 - [R_{cc}^2 j_1(kR_{cc})/k]^2$ times the head-group neutron scattering contrast (this introduces another adjustable parameter with which to fit the experimental data). Finally, note that the scattering off of free monomers is also neglected. A more realistic charged-rod

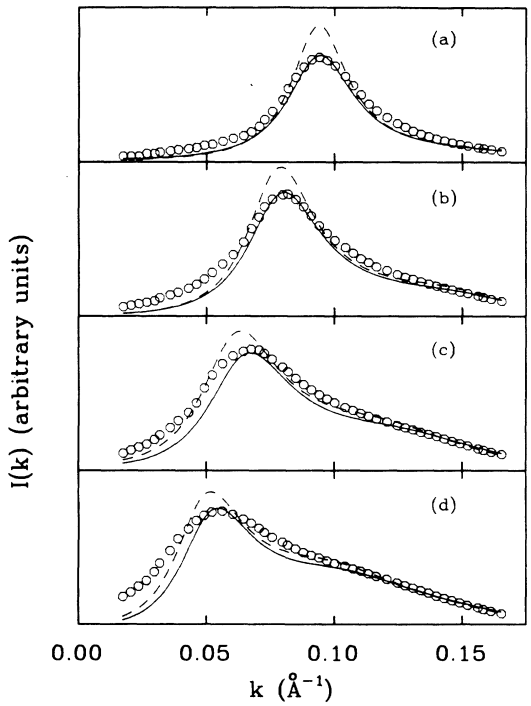

FIG. 9. Comparison with experimental small angle neutron scattering intensities for micellar systems [Ref 2(b)]. See Table I for details. Each panel shows the experimental points of Ref. 2(b) (open circles), the MSA-HNC approximation using the reported physical parameters of Ref. 2(b) (— — —) and the refit MSA-HNC approximation (——).

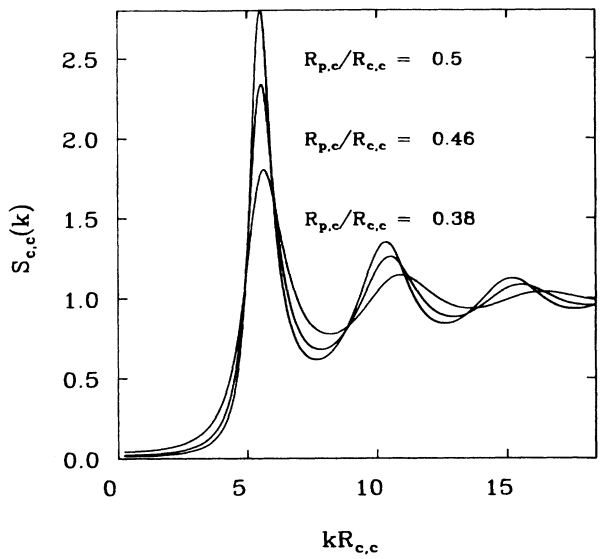

FIG. 10. The effect of nonadditive core diameters on $S_{cc}(k)$ for a dense micelle-sized system in water at 310 K with R_{cc} = 48.5 Å, z_c = 75e, ξ_{cc} = 0.25, and there was no added salt.

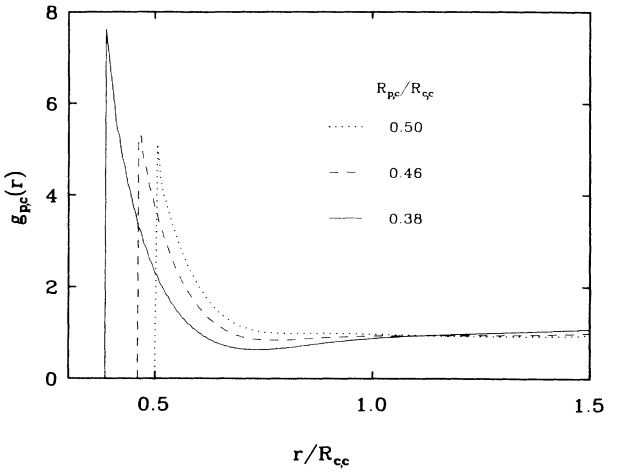

FIG. 11. The counter-ion density [i.e., $g_{pc}(r)$] for the cases shown in Fig. 8.

model will give a nonzero form factor, thus adding further corrections to the theoretical structure factor.

Reinterpretation of the micellar charge, density, and size (see Table I) shows that (i) on the average, 80—90% of the monomers are micellized, and (ii) the refitted micellar charge is consistently less than those reported by Chen. Note, that no explicit CMC correction has been introduced, and thus, the effective CMC is slightly different than Chen's. In addition, in contrast with dilute colloidal suspensions, there is a strong renormalization of charge [cf. Eq. (2.32)] which can be accurately estimated by Eq. (2.38).

Finally, the effects of nonadditivity are examined in Figs. 10 and 11 and Table II for micelle-sized particles. Note that the density is roughly twice that studied by Chen *et al.* The choice of the degree of nonadditivity is based on Chen's geometric model of a spherical micelle and allows for the counter-ion to either not penetrate the head-group region at all (additive case) or penetrate up to the core region ($R_{pc}/R_{cc} \sim 0.385$). A large change in the magnitude of S_{cc} (cf. Fig. 10) as well as in the effective charge (cf. Table II) are observed. The decrease in the effective charge can be understood in terms of the increased local density of counter-ions as shown in Fig. 11. Of course, g_{pc} should increase since the p-c Coulomb attrac-

TABLE I. Summary of some micelle results shown in Fig. 7.

Case	ξ_{cc}	R_{cc} (Å)	z_c	z_c^{eff} Calc.	z_c^{eff} Eq. (2.38)	% Micellized	λR_{cc}	$\nu_0 R_{cc}$
				Fitted Parameters of Ref. 2(b)				
a	0.14	48.4	75.0	30.8	24.6	99.93[a]	4.1[b]	
b	0.07	46.2	63.0	25.2	26.3	96.51	2.8	
c	0.03	45.1	57.0	22.8	27.8	79.99	2.1	
d	0.015	44.3	53.0	20.7	28.6	78.41	1.7	
				MSA-HNC, Using Fitted Parameters of Ref. 2(b)				
a	0.14	48.4	75.0	18.6	18.5	99.93	6.13	0.160
b	0.07	46.2	63.0	20.7	20.6	96.51	4.10	0.093
c	0.03	45.1	57.0	22.6	22.5	79.99	3.06	0.039
d	0.015	44.3	53.0	25.8	25.6	78.41	2.14	0.025
				MSA-HNC, Refitting Experimental Data of Ref. 2(b)				
a	0.131	47.4	69.0	16.85	16.76	91.9	6.24	0.138
b	0.068	45.2	57.7	18.87	18.90	91.7	4.11	0.092
c	0.032	43.3	48.2	19.63	20.59	81.0	2.92	0.054
d	0.016	42.8	46.0	22.75	22.72	80.5	2.05	0.042

[a]This reflects the small difference between the total amount of LDS and that contained in the micelles reported in Ref. 2(b).
[b]In the calculation of Ref. 2(b), the ions in the CMC and the fraction of counter-ions corresponding to the effective micellar charge were included in the calculation of the screening length.

TABLE II. The effect of nonadditivity for micelles. For all three cases, $z_c = 75e$, $R_{cc} = 48.5$ Å, and $\rho_c R_{cc}^3 = 0.477$.

	z_c^{eff}		
R_{pc}/R_{cc}	Calc.	Eq. (2.38)	$\nu_0 R_{cc}$
0.50	15.3	15.3	0.450
0.46	11.8	11.7	0.527
0.385	7.40	7.37	0.723

tion will be larger. In addition, note that the approximate expression for the effective charge, cf. Eq. (2.38), does quite well (cf. Table II).

IV. CONCLUDING REMARKS

In this work, we have shown that the MSA-HNC approximation was both easy to implement, and, where comparison was possible, gave results which were in good agreement with the full multicomponent HNC approximation. The various partial structure factors and correlation functions had a reasonable form even for extremely large charge asymmetry.

A number of new features were discussed. In particular, in colloids, we predict a second melting of colloidal crystals if the colloidal charge is increased enough. In micellar systems, we have shown that the effects of partial micellization or counter-ion—micelle inter-penetrability can have large effects on the calculated structure factors. However, the simple modification of the Verwey-Overbeek effective charge used to calculate the macro-ion—macro-ion structure factor [cf. Eq. (2.38)] seems to work quite well.

In highly charged systems, the counter-ion correlations contain a number of very different length scales (see, e.g., Fig. 6). The short length scale describes the distribution of counter-ions around a given macro-ion, which are reminiscent of the ionic distributions found around an electrode.[19] The longer length scale describes the correlations between the macro-ions (or those induced by them) and are not present in theories of electrodes (or equivalently of macro-ionic the solutions at infinite dilution). It is possible that the difficulty in numerically solving the full multicomponent HNC approximation lies in the nonlinear interplay of these different scales (here they were handled analytically within the MSA). In the future, we will report on other analytic and numerical approximations on the HNC equations which can overcome this problem.

ACKNOWLEDGMENTS

We thank L. Blum, S.-H. Chen and E. Y. Sheu for helpful discussions. A portion of this work was supported by the National Science Foundation, by the Alfred P. Sloan Research Foundation, and by the Camille and Henry Dreyfus Foundation. One of us (S.K.) gratefully acknowledges the Natural Sciences and Engineering Research Council of Canada for support.

[1](a) D. W. Schaefer and B. J. Berne, Phys. Rev. Lett. **32**, 1110 (1974); (b) J. C. Brown, P. N. Pusey, J. W. Goodwin, and R. H. Ottewill, J. Phys. A **8**, 664 (1978); (c) N. A. Clark and B. J. Ackerson, Phys. Rev. Lett. **44**, 1005 (1980); Physica (Utrecht) **118A**, 221 (1983); (d) D. W. Schaefer, J. Chem. Phys. **66**, 3980, (1977).

[2](a) E. Y. Sheu, C.-F. Wu, S.-H. Chen, and L. Blum, Phys. Rev. A **32**, 3807 (1985); (b) S.-H. Chen, *Physics of Amphiphiles: Micelles, Vescicles and Microemulsions,* edited by V. Degiorgio and M. Corti (Elsevier, New York, 1985), p. 281; (c) Y.-S. Chao, E. Y. Sheu, and S.-H. Chen, J. Phys. Chem. **89**, 4862 (1985); (d) G. Senatore and L. Blum, J. Phys. Chem. **89**, 2676 (1985); (e) M. Medina-Noyola, J. Chem. Phys. **77**, 1428 (1982).

[3](a) M. S. Wertheim, Phys. Rev. Lett. **10**, 321 (1963), J. L. Lebowitz, Phys. Rev. **133**, 895 (1964); (b) E. Waisman and J. L. Lebowitz, J. Chem. Phys. **52**, 4307 (1970), **56**, 3086, 3093 (1972); (c) L. Blum, Mol. Phys. **30**, 1529 (1975); (d) L. Blum and J. S. Høye, J. Phys. Chem. **81**, 1311 (1977), Mol. Phys. **35**, 299 (1978); (e) K. Hiroike, Mol. Phys. **33**, 1195 (1977); (f) E. Waisman, Mol. Phys. **25**, 45 (1973); (g) J. S. Høye and G. Stell, Mol. Phys. **32**, 195, 209 (1976); (h) J. S. Høye and L. Blum, J. Stat. Phys. **16**, 399 (1977); **19**, 317 (1978); L. Blum, J. Stat. Phys. **22**, 661 (1980).

[4](a) J.-P. Hansen and J. B. Hayter, Mol. Phys. **46**, 651 (1982); (b) J. B. Hayter, Faraday Discuss. Chem. Soc. **76**, 7 (1983); (c) J. B. Hayter and J. Penfold, Mol. Phys. **42** 109 (1981); also see Ref. 3(h).

[5]D. Ronis, J. Chem. Phys. **81**, 2749 (1984).

[6]S. Khan and D. Ronis, Mol. Phys. **60**, 637 (1987).

[7]M. J. Gillan, J. Phys. C: Sol. State Phys. **7**, L1 (1974); A. H. Narten, L. Blum, and R. H. Fowler, J. Chem. Phys. **60**, 3378 (1974).

[8](a) G. N. Patey, J. Chem. Phys. **72**, 5763 (1980); (b) A. Vrij, J. Chem. Phys. **72**, 3735 (1980); (c) G. Nagele, R. Klein, and M. Medina-Noyola, J. Chem. Phys. **83**, 2560 (1985).

[9]L. Belloni, Chem. Phys. **99**, 43 (1985). Note that Belloni uses c to denote the counter-ion and p to denote the macro-ion; the reverse is true here.

[10]D. Bratko, H. L. Friedman, and E. C. Zhong, J. Chem. Phys. **85**, 377 (1986); D. Bratko, H. L. Friedman, S.-H. Chen, and L. Blum, Phys. Rev. A **34**, 2215 (1986).

[11]E. J. W. Verwey and J. Th. G. Overbeek, *Theory of the Stability of Lyophobic Colloids* (Elsevier, New York, 1948).

[12]S. Alexander, P. M. Chaiken, P. Grant, G. J. Morales, P. Pincus, and D. Hong, J. Chem. Phys. **80**, 5776 (1984).

[13]J. P. Hansen and L. Verlet, Phys. Rev. **184**, 150 (1969).

[14]J. M. J. Van Leeuwen, J. Groenenveld, and J. de Boer, Physica (Utrecht) **25**, 792 (1959).

[15]M. J. Gillan, Mol. Phys. **38**, 1781 (1979).

[16]F. Stillinger and R. Lovett, J. Chem. Phys. **49**, 1991 (1968).

[17]D. Blankschtein, G. M. Thurston, and G. B. Benedek, J. Chem. Phys. **85**, 7268 (1986).

[18]E. Y. Sheu and S.-H. Chen, private communication.

[19]For a review, see S. L. Carnie and G. M. Torrie, Adv. Chem. Phys. **54**, 141 (1984); for nonplanar electrodes, see M. Lozada-Cassou, J. Phys. Chem. **87**, 3729 (1983); R. Bacquet and P. J. Rossky, J. Phys. Chem. **88**, 2660 (1984); C. S. Murthy, R. Bacquet, and P. J. Rossky, J. Phys. Chem. **89**, 701 (1985).